Journal of Computational Physics 228 (2009) 1000–1016

Contents lists available at ScienceDirect

Journal of Computational Physics

journal homepage: www.elsevier.com/locate/jcp

A low frequency stable plane wave addition theorem

Ignace Bogaert [a,*], Femke Olyslager [a]

[a] Department of Information Technology (INTEC), Ghent University, Sint-Pietersnieuwstraat 41, B-9000 Ghent, Oost-Vlaanderen, Belgium

ARTICLE INFO

Article history:
Received 26 February 2008
Received in revised form 5 September 2008
Accepted 6 October 2008
Available online 25 October 2008

Keywords:
Fast multipole method
Diagonal translation
Stable at LF

ABSTRACT

The multilevel fast multipole algorithm (MLFMA) is a well known and very successful method for accelerating the matrix-vector products required for the iterative solution of Helmholtz problems. The MLFMA has an important drawback, namely its inability to handle scattering problems with a lot of subwavelength detail due to the low frequency (LF) breakdown of the MLFMA. There is a need to extend the MLFMA to LF, since alternative methods are less efficient (multipole methods) or hard to implement (spectral methods). In this paper a new addition theorem will be developed that does not suffer from an LF breakdown. Instead it suffers from a high-frequency (HF) breakdown. The new method relies on a novel set of distributions, the so-called pseudospherical harmonics, closely related to the spherical harmonics. These allow the discretization points and translation operators to be calculated in closed form. Hence the method presented in this paper allows the easy implementation of a method that is stable at LF. Furthermore, a combination of the traditional MLFMA and the new method allows for the construction of a broadband MLFMA.

1. Introduction

Integral equations containing the Green function of the Helmholtz equation are a very important class of problems in fields such as acoustics and electromagnetics. Usually these equations are discretized by means of the method of moments [1]. The discretized equation can then be interpreted as a linear system of dimension N, where N is the number of basis functions used to discretize the integral equation. A direct solution (for example by means of an LU decomposition) requires $\mathcal{O}(N^3)$ operations, therefore this approach rapidly becomes impractical for increasing N. Iterative solution methods can be used to improve on this situation. They only require P matrix-vector multiplications to gradually converge to a solution. If the problem is well conditioned, $P << N$. Of course the matrix-vector multiplications still require $\mathcal{O}(N^2)$ operations, such that solving the problem requires $\mathcal{O}(PN^2)$ operations.

A further reduction in operations count can be achieved by applying a so-called fast multipole method (FMM). These methods reduce the complexity of a matrix-vector multiplication from $\mathcal{O}(N^2)$ to $\mathcal{O}(N)$ or $\mathcal{O}(N\ln N)$. The MLFMA is one such method, and is very efficient for structures that do not contain much subwavelength geometrical detail. For example, simulations with tens of millions of unknowns have been performed with parallelized versions of the MLFMA [2,3]. However, the efficient simulation of structures that do contain a lot of subwavelength geometrical detail is prevented by a phenomenon called the LF breakdown. The LF breakdown of the MLFMA [4–6] is not of mathematical origin but is caused by the inevitable numerical roundoff error on a finite-precision computer. Hence, broadband simulations require the integration of the MLFMA with another method that efficiently takes care of the subwavelength geometrical detail. In [7] the MLFMA is used in conjunction with a multipole based method. Although this multipole based method achieves computational complexity $\mathcal{O}(N)$, the translations in this method are not diagonal, resulting in a relatively slow algorithm. In [8,9], an

* Corresponding author. Tel.: +32 9 26 43354; fax: +32 9 2649969.
E-mail address: Ignace.Bogaert@intec.ugent.be (I. Bogaert).

0021-9991/$ - see front matter © 2008 Elsevier Inc. All rights reserved.
doi:10.1016/j.jcp.2008.10.022

FMM based on the spectral representation of the Green function is introduced, which leads to diagonal translation operators that are stable for all frequencies. Unfortunately the spectral representation of the Green function converges in only one halfspace, thereby imposing the need for six radiation patterns. This causes the factor hidden in the $\mathcal{O}(N)$ or $\mathcal{O}(N \ln N)$ to be quite large. Additionally in [10], where a similar technique is used, it is stated that "the CPU time requirements of the scheme are minimized when HF techniques are used wherever possible". The term 'HF techniques' refers to the MLFMA.

All this obviates the need for an addition theorem that is stable at LF and similar to the one used in the MLFMA. The first steps in the search for such an addition theorem were taken in the uniform multilevel fast multipole algorithm (UMLFMA) [11]. In the UMLFMA, the integration path is shifted into the complex plane so as to include more near-field information in the radiation pattern. However, the translation operators have to be calculated numerically. Also, the complex shift has to be tweaked manually since no clear prescription is known [6]. Recently a novel method, the nondirective stable plane wave multilevel fast multipole algorithm (NSPWMLFMA [12]), has been proposed which does not suffer from these drawbacks. It also uses a shift into the complex plane but instead of numerically constructing the translation operators, they are obtained from a QR decomposition of an analytically known matrix. The discretization points for the radiation patterns are also selected using QR decomposition, which guarantees a high accuracy. However, the fact that the discretization points are selected using the QR algorithm also destroys any symmetry properties of the discretization points. Therefore, inter- and anterpolations must be done using dense matrices, making these operations a more costly part of the algorithm for high accuracies. In this paper a novel addition theorem will be derived that is completely known in closed form, i.e. explicit formulas for the translation operators and discretization points will be given. As in the UMLFMA, a shift of the integration path into the complex plane will then be used to make it numerically stable at LF. A heuristic algorithm for the calculation of the complex shift will be given and the limits to the error-controllability will be explored. In addition it will be shown that the inter- and anterpolations can be performed efficiently using FFTs.

In this paper, the norm of a vector is denoted by the same symbol as the vector, but without boldface: $v = \sqrt{\boldsymbol{v} \cdot \boldsymbol{v}}$. Unit vectors are denoted with a hat $\hat{\boldsymbol{v}} = \frac{\boldsymbol{v}}{v}$. An asterisk denotes complex conjugation. In the MLFMA, the two most important vectors are the translation vector $\boldsymbol{r}_T$ and the vector $\boldsymbol{r}_A$ (see Fig. 1). The vector $\boldsymbol{r}_A = \boldsymbol{r}_a - \boldsymbol{r}_d$ actually consists of a part coming from the aggregation $\boldsymbol{r}_a = \boldsymbol{R}_1 - \boldsymbol{r}_1$ and a part from the disaggregation $\boldsymbol{r}_d = \boldsymbol{R}_2 - \boldsymbol{r}_2$. The translation vector $\boldsymbol{r}_T$ is given by $\boldsymbol{R}_2 - \boldsymbol{R}_1$ such that $\boldsymbol{r} = \boldsymbol{r}_2 - \boldsymbol{r}_1 = \boldsymbol{r}_A + \boldsymbol{r}_T$.

2. A general form of the addition theorem of the MLFMA

The addition theorem of the MLFMA is well known [13]. However, it is not unique in its usefulness to FMM as will be proven in Subsection 2.1. In fact there may be an infinite number of possible addition theorems, all of which equally valid for the construction of an FMM (although they might be numerically unstable). In the following subsections three special cases will be discussed. Two of them will be shown to reduce to known results from the literature, among which the usual addition theorem of the MLFMA. These two special cases do not allow stable translation operators for LF. The third case is based on a novel set of distributions, the so-called pseudospherical harmonics, and will be used in the next sections to construct LF-stable translation operators.

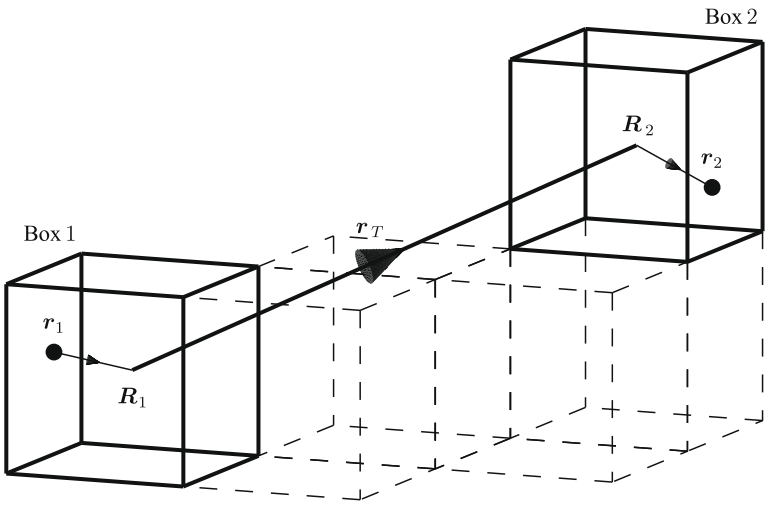

Fig. 1. A typical configuration in the MLFMA.

2.1. A more general addition theorem

The starting point of the derivation is the addition theorem for the spherical Hankel function of the zeroth order and second kind

$$h_0^{(2)}(kr) = \frac{e^{-jkr}}{-jkr} = \sum_{l=0}^{\infty}(-1)^l(2l+1)j_l(kr_A)h_l^{(2)}(kr_T)P_l(\hat{\boldsymbol{r}}_A\cdot\hat{\boldsymbol{r}}_T), \tag{1}$$

which converges absolutely if $r_T > r_A$. This equation can be found in [14], Eqs. (10.1.5) and (10.1.6). The function $P_l(\cdot)$ is the Legendre polynomial of degree l, while $Y_{l,m}(\theta,\phi)$ is a spherical harmonic of degree l and order m. Both are defined in Appendix A. In the following, the infinite sum (1) will be truncated after L, i.e. terms with $l > L$ will be neglected. The truncation bound L is determined such that the relative error introduced by the truncation of (1) is lower than a given threshold ϵ

$$(2L+3)j_{L+1}(kr_A)|h_{L+1}^{(2)}(kr_T)| \leqslant \epsilon|h_0^{(2)}(kr_T)|. \tag{2}$$

To avoid the possibility of using (2) near a zero of the spherical Bessel function, the condition $L+1 > kr_A$ should be added. Now consider any set of functions $f_{l,m}(\theta,\phi)$ such that the following property holds

$$\int_D f_{l,m}(\theta,\phi)Y_{l',m'}^*(\theta,\phi)w(\theta,\phi)\mathrm{d}\theta\mathrm{d}\phi = \delta_{l,l'}\delta_{m,m'}, \tag{3}$$

for some integration domain D and weight distribution $w(\theta,\phi)$. By means of (3), (62) and the expansion of a plane wave

$$e^{-j\boldsymbol{k}(\theta,\phi)\cdot\boldsymbol{r}_A} = \sum_{l=0}^{\infty}(2l+1)j^{-l}j_l(kr_A)P_l(\hat{\boldsymbol{k}}(\theta,\phi)\cdot\hat{\boldsymbol{r}}_A), \tag{4}$$

the spherical Hankel function $h_0^{(2)}(kr)$ can be written as

$$h_0^{(2)}(kr) \approx \frac{1}{4\pi}\int_D e^{-j\boldsymbol{k}(\theta,\phi)\cdot\boldsymbol{r}_A}T(k\boldsymbol{r}_T,\theta,\phi)w(\theta,\phi)\mathrm{d}\theta\mathrm{d}\phi, \tag{5}$$

with

$$T(k\boldsymbol{r}_T,\theta,\phi) = 4\pi\sum_{l=0}^{L}\sum_{m=-l}^{l}j^{-l}h_l^{(2)}(kr_T)f_{l,m}(\theta,\phi)Y_{l,m}^*(\theta_T,\phi_T), \tag{6}$$

and $\boldsymbol{k}(\theta,\phi) = k\hat{\boldsymbol{k}}(\theta,\phi)$, with $\hat{\boldsymbol{k}}(\theta,\phi) = \cos\phi\sin\theta\hat{\boldsymbol{x}} + \sin\phi\sin\theta\hat{\boldsymbol{y}} + \cos\theta\hat{\boldsymbol{z}}$ and k the wavenumber. Three valid choices for $f_{l,m}$, D and w will now be given. The first two have already been described in the literature and are widely known and used. However, no simple method exists to make these two translation operators numerically stable at LF. The third choice uses a novel set of functions, the so-called pseudospherical harmonics, for $f_{l,m}$. In contrast to the first two choices, the addition theorem corresponding to this third choice can be made numerically stable for LF.

2.2. Choice 1: the MLFMA

By choosing

$$f_{l,m}(\theta,\phi) = Y_{l,m}(\theta,\phi), \tag{7}$$
$$w(\theta,\phi) = \sin\theta, \tag{8}$$
$$D = [0,2\pi]\otimes[0,\pi], \tag{9}$$

Eq. (5) reduces to the traditional addition theorem of the MLFMA

$$h_0^{(2)}(kr) \approx \frac{1}{4\pi}\int_0^{2\pi}\int_0^{\pi}e^{-j\boldsymbol{k}(\theta,\phi)\cdot\boldsymbol{r}_A}T(k\boldsymbol{r}_T,\theta,\phi)\sin\theta\mathrm{d}\theta\mathrm{d}\phi, \tag{10}$$

with the translation operator being defined as

$$T(k\boldsymbol{r}_T,\theta,\phi) = \sum_{l=0}^{L}(2l+1)j^{-l}h_l^{(2)}(kr_T)P_l(\hat{\boldsymbol{k}}(\theta,\phi)\cdot\hat{\boldsymbol{r}}_T). \tag{11}$$

The addition theorem of the MLFMA is usually discretized using Gauss–Legendre quadrature points [15].

2.3. Choice 2: the MLFMA with uniform discretization

In [16], Sarvas presented an approach corresponding to the following choices

$$f_{l,m}(\theta,\phi) = \frac{1}{2}Y_{l,m}(\theta,\phi)|\sin\theta|, \tag{12}$$
$$w(\theta,\phi) = 1, \tag{13}$$
$$D = [0,2\pi]\otimes[0,2\pi], \tag{14}$$

Proving that this choice satisfies (3) is straightforward when given Eq. (60) of Appendix A. The integration domain runs over a full period of the integrand in both θ and ϕ. Therefore the integration in (5) can be efficiently performed using uniformly sampled points in both the θ and ϕ direction provided that the Fourier series of $f_{l,m}(\theta,\phi)$ in both θ and ϕ are truncated at bandwidth L (a smoothing operation).

$$\theta_{n_\theta} = \frac{2\pi}{N_\theta} n_\theta, \forall n_\theta \in [1, N_\theta], \tag{15}$$

$$\phi_{n_\phi} = \frac{2\pi}{N_\phi} n_\phi, \forall n_\phi \in [1, N_\phi], \tag{16}$$

with $N_\theta = 2L+1$. The uniform sampling allows inter- and anterpolations to be done entirely with FFTs. Moreover if N_ϕ is even, Eq. (60) allows a reduction of the number of discretization points by a factor two, therefore $N_\phi = 2L+2$.

2.4. Choice 3: pseudospherical harmonics

We propose the following novel choice

$$f_{l,m}(\theta,\phi) = \begin{cases} \frac{1}{2} U_{l,m}(\theta,\phi)\sin\theta \forall m \geqslant 0 \\ \frac{1}{2}(-1)^m U^*_{l,-m}(\theta,\phi)\sin\theta \forall m < 0 \end{cases}, \tag{17}$$

$$w(\theta,\phi) = 1, \tag{18}$$

$$D = [0, 2\pi] \otimes [0, 2\pi]. \tag{19}$$

The $U_{l,m}(\theta,\phi)$ are distributions which are conveniently called "the pseudospherical harmonics", defined in Appendix B. Proving that this choice satisfies (3) is equivalent to proving Theorem B.1 as is done in Appendix B. As in the previous subsection, the integration in (5) can be efficiently performed using a uniform discretization, this time with $N_\phi = N_\theta = 2L_d + 1$. The number of points is calculated based on L_d, not L itself, for reasons that will be explained in Section 3. Also, it will become clear in Section 4 that a reduction of the number of discretization points, as was possible in Subsection 2.3, is not possible anymore. Therefore, there is no need to make the number of points in the ϕ direction even, hence $N_\phi = 2L_d + 1$ A uniform discretization again necessitates a smoothing of $U_{l,m}(\theta,\phi)\sin\theta$ to bandwidth L_d. Therefore the Fourier spectrum of $U_{l,m}(\theta,\phi)\sin\theta$ will be determined in Section 3. The special properties of the Fourier spectrum of $U_{l,m}(\theta,\phi)\sin\theta$ will then for the first time allow the construction of analytically known LF-stable translation operators.

3. The pseudospherical harmonics as a fourier series

The addition theorem following from the choice for $f_{l,m}$, D and w in Subsection 2.4 is

$$h_0^{(2)}(kr) \approx \frac{1}{4\pi} \int_0^{2\pi} \int_0^{2\pi} e^{-j\mathbf{k}(\theta,\phi)\cdot\mathbf{r}_A} T(k\mathbf{r}_T, \theta, \phi) \mathrm{d}\theta \mathrm{d}\phi, \tag{20}$$

with the translation operator

$$T(k\mathbf{r}_T, \theta, \phi) = 2\pi \sin\theta \sum_{l=0}^{L} j^{-l} h_l^{(2)}(kr_T) \sum_{m=0}^{l} s_m [Y^*_{l,m}(\theta_T,\phi_T) U_{l,m}(\theta,\phi) + Y_{l,m}(\theta_T,\phi_T) U^*_{l,m}(\theta,\phi)], \tag{21}$$

with $s_m = 1 - \frac{1}{2}\delta_{m,0}$ and the fact that $U^*_{l,0}(\theta,\phi) = U_{l,0}(\theta,\phi)$. The uniform discretization proposed in Subsection 2.4 allows the exact integration of a function with bandwidth $2L_d$. Because the translation operator shares this bandwidth with the plane wave in (20), it must be smoothed to a bandwidth L_d. In practice, this amounts to calculating the Fourier series of $U_{l,m}(\theta,\phi)\sin\theta$ for $m \geqslant 0$, i.e. writing it as

$$U_{l,m}(\theta,\phi)\sin\theta = e^{jm\phi} \sum_{n=-\infty}^{\infty} u^n_{l,m} e^{jn\theta} \tag{22}$$

and truncating the summation to the range $[-L_d, L_d]$. It is worthwhile to point out that property (66) of Appendix B yields a condition on the Fourier coefficients, namely

$$u^{-n}_{l,m} = (-1)^m u^n_{l,m}. \tag{23}$$

The calculation of $u^n_{l,m}$ can be done by using Theorem C.2

$$U_{l,m}(\theta,\phi)\sin\theta = K_{l,m} e^{jm\phi} \sin^{m+1}\theta \frac{2^{m+1}}{\sqrt{\pi}} \sum_{p=0}^{\infty} \lambda^p_{l,m} \sin[(l+m+2p+1)\theta]. \tag{24}$$

Theorem C.2 is proven and $K_{l,m}$ is defined in Appendix A, while the coefficient $\lambda^p_{l,m}$ is defined in Appendix C. It is shown in Theorem C.3 that if $\lambda^p_{l,m}$ is interpreted as $\lim_{x\to p}\lambda^x_{l,m}$, then

$$\lambda^p_{l,m} = -\lambda^{-p-l-m-1}_{l,m}. \tag{25}$$

Furthermore, using (82), it is easily seen that

$$\lambda^p_{l,m} = 0 \forall p \in [-l-m, -1]. \tag{26}$$

As a consequence Eq. (24) can be rewritten as

$$U_{l,m}(\theta,\phi)\sin\theta = -jK_{l,m}e^{jm\phi}\sin^{m+1}\theta\frac{2^m}{\sqrt{\pi}}\sum_{p=-\infty}^{\infty}\lambda^p_{l,m}e^{j(l+m+2p+1)\theta}. \tag{27}$$

Because $m \geqslant 0$ in (21), it is possible to expand $\sin^{m+1}\theta$ using the binomial theorem. Absorbing the result into the summation over p yields the following closed form

$$u^n_{l,m} = \begin{cases} \frac{1}{2}\frac{K_{l,m}(-j)^m}{\sqrt{\pi}}\sum_{q=0}^{m+1}(-1)^{m-q}\binom{m+1}{q}\lambda^{\frac{n-l}{2}-q}_{l,m} & \forall n-l \text{ even} \\ 0 & \forall n-l \text{ odd} \end{cases}, \tag{28}$$

with the binomial coefficient

$$\binom{m+1}{q} = \frac{(m+1)!}{q!(m+1-q)!}. \tag{29}$$

The $u^n_{l,m}$ satisfy the following curious property

Theorem 3.1. *For any integer n, $l \geqslant 0$ and $m \in [0, l]$ the following holds*

$$u^n_{l,m} = 0 \forall l > |n|. \tag{30}$$

Proof. The inequality $l > |n|$ and the summation bounds for q in Eq. (28) yield the following two inequalities

$$-l < \frac{n-l}{2} < 0, \tag{31}$$

$$-m-1 \leqslant -q \leqslant 0. \tag{32}$$

The sum of Eqs. (31) and (32) yields

$$-l-m-1 < \frac{n-l}{2} - q < 0, \tag{33}$$

which proves by means of Eq. (26), that all the terms in summation (28) are zero, concluding the proof. □

It can also be verified that $u^n_{l,m}$ diverges as a function of n if $m > 2$. However, as mentioned before, the pseudospherical harmonics are distributions, therefore (22) does not have to converge. Provided the distribution is integrated with a function that has a Fourier spectrum that decays fast enough to compensate the divergence, a well-defined result is obtained. Equation (28) makes it easy to calculate the smoothed translation operator

$$\widetilde{T}(k\mathbf{r}_T,\theta,\phi) = 2\pi\sum_{n=-L_d}^{L_d}\sum_{m=0}^{L}\sum_{l=m}^{L}j^{-l}h^{(2)}_l(kr_T)s_m \times [Y^*_{l,m}(\theta_T,\phi_T)e^{jm\phi} + Y_{l,m}(\theta_T,\phi_T)e^{-jm\phi}]u^n_{l,m}e^{jn\theta}, \tag{34}$$

$$= \sum_{n=-L_d}^{L_d}\sum_{m=-L}^{L}\left[2\pi\sum_{l=|m|}^{L}j^{-l-m+|m|}h^{(2)}_l(kr_T)Y^*_{l,m}(\theta_T,\phi_T)u^n_{l,|m|}\right]e^{jn\theta}e^{jm\phi}. \tag{35}$$

Using Theorem 3.1, the innermost summation can be truncated

$$\widetilde{T}(k\mathbf{r}_T,\theta,\phi) = \sum_{n=-L_d}^{L_d}\sum_{m=-L}^{L}\underbrace{\left[2\pi\sum_{l=|m|}^{\min(|n|,L)}j^{-l-m+|m|}h^{(2)}_l(kr_T)Y^*_{l,m}(\theta_T,\phi_T)u^n_{l,|m|}\right]}_{t_{n,m}}e^{jn\theta}e^{jm\phi}. \tag{36}$$

The two outer sums can be performed using the FFT algorithm, due to the uniform discretization. Assuming that L_d does not differ too much from L, the calculation of the smoothed translation operator $\widetilde{T}(k\mathbf{r}_T,\theta,\phi)$ requires the evaluation of $u^n_{l,m}$ in $\mathcal{O}(L^3)$ different arguments. The evaluation of $u^n_{l,m}$ itself costs $\mathcal{O}(L)$ operations hence the calculation of the smoothed translation operator is dominated by the $\mathcal{O}(L^4)$ scaling of calculating the various $u^n_{l,m}$. Although this problem is not that severe because the $u^n_{l,m}$ can be reused for all the different translation directions, in Appendix D we supply a more efficient recursive calculation method that yields an $\mathcal{O}(L^3)$ calculation of all required $u^n_{l,m}$.

Using the uniform discretization from Eqs. (15) and (16), the smoothed translation operator can be directly discretized

$$h_0^{(2)}(kr) \approx \frac{\pi}{N_\theta N_\phi} \sum_{n_\theta=1}^{N_\theta} \sum_{n_\phi=1}^{N_\phi} \widetilde{T}(k\boldsymbol{r}_T, \theta_{n_\theta}, \phi_{n_\phi}) e^{-j\boldsymbol{k}(\theta_{n_\theta}, \phi_{n_\phi})\cdot \boldsymbol{r}_A}. \tag{37}$$

An error analysis will now be performed to control the discretization error and determine the value of L_d. In this analysis the effects of roundoff error will be ignored, a subject being studied in the next section. The uniform discretization exactly integrates every function of bandwidth $2L_d$. Because in the translation operator, the spectrum of pseudospherical harmonics has been truncated to bandwidth L_d, the orthogonality property (B.1) between pseudospherical harmonics and spherical harmonics holds after discretization if $l_2 \leqslant L_d$. The plane wave, however, contains spherical harmonics with all orders, such that this inequality will be violated. Therefore, (37) becomes

$$h_0^{(2)}(kr) \approx \sum_{l=0}^{L} (-1)^l (2l+1) j_l(kr_A) h_l^{(2)}(kr_T) P_l(\hat{\boldsymbol{r}}_A \cdot \hat{\boldsymbol{r}}_T) + \frac{\pi}{N_\theta N_\phi} \sum_{n_\theta=1}^{N_\theta} \sum_{n_\phi=1}^{N_\phi} \widetilde{T}(k\boldsymbol{r}_T, \theta_{n_\theta}, \phi_{n_\phi}) \times \sum_{l=L_d+1}^{\infty} (2l+1) j^{-l} j_l(kr_A) P_l(\hat{\boldsymbol{k}}(\theta_{n_\theta}, \phi_{n_\phi}) \cdot \hat{\boldsymbol{r}}_A). \tag{38}$$

Since L has been chosen to satisfy (1) with an accuracy ϵ, we can conclude that the second term must be reduced below the same accuracy threshold to safeguard the error-controllability of the method. In the MLFMA, this condition is automatically satisfied because the Fourier series of spherical harmonics converges. In the method proposed here, however, the diverging nature of the Fourier series of the pseudospherical harmonics blows up the second term. However, it can be suppressed by choosing L_d sufficiently large. Indeed, without taking into account numerical roundoff error, it is possible to make this term arbitrarily small because the lowest order spherical Bessel function is $j_{L_d+1}(kr_A)$, which converges super-exponentially if $L_d > kr_A$. For the same reason the value of L_d approaches L if the frequency drops. For situations where kr_A has a value around or above unity, however, the difference between L_d and L can be significant. Numerical experiments can be used to determine a suitable value for L_d by starting at $L_d = L + 1$ and gradually increasing L_d. For this the translation operator with translation direction $\hat{\boldsymbol{e}}_x$ should be used. This choice can be understood by looking at translations close to the z-axis. Indeed, for these translations the factor $\sin^{|m|}\theta_T$ contained within $Y^*_{L,m}(\theta_T, \phi_T)$ becomes dominant over the diverging behavior of $u^n_{l,m}$. Hence, their Fourier spectrum does not increase as fast as the Fourier spectrum of other translation operators. For translations far enough away from the z-axis, this suppression of the divergence becomes less and less strong, and disappears completely in the xy-plane (where $\theta_T = \frac{\pi}{2}$). Therefore the translations in the xy-plane should have approximately the fastest increasing Fourier spectrum, yielding a worst case scenario for the determination of L_d. To avoid having to take into account the various possible $\boldsymbol{r}_A$, the following inequality is useful

$$\left| \sum_{m=-l}^{l} a_{l,m} Y_{l,m}(\theta, \phi) \right| \leqslant \sqrt{\frac{2l+1}{4\pi}} \sqrt{\sum_{m=-l}^{l} |a_{l,m}|^2}. \tag{39}$$

As a consequence, when $a_{l,m}$ is defined as

$$a_{l,m} = j^{-l} j_l(kr_A) \frac{4\pi^2}{N_\theta N_\phi} \sum_{n_\theta=1}^{N_\theta} \sum_{n_\phi=1}^{N_\phi} \widetilde{T}(kr_T \hat{\boldsymbol{e}}_x, \theta_{n_\theta}, \phi_{n_\phi}) Y_{l,m}(\theta_{n_\theta}, \phi_{n_\phi}), \tag{40}$$

the following inequality must be satisfied to obtain a relative accuracy ϵ

$$\sum_{l=L_d+1}^{\infty} \sqrt{\frac{2l+1}{4\pi}} \sqrt{\sum_{m=-l}^{l} |a_{l,m}|^2} < \epsilon |h_0^{(2)}(kr)|. \tag{41}$$

4. A normalized translation operator

The translation operator derived in the previous section is neither LF-stable nor HF-stable. The instability for the HF case is caused by the exponential divergence of $u^n_{l,m}$ as a function of n and cannot be easily remedied. However, for the LF case L becomes fixed as the frequency drops, and the numerical instability associated with the diverging $u^n_{l,m}$ becomes fixed as well. The instability due to the super-exponential increase of the spherical Hankel functions, on the other hand, becomes more and more of a problem as the frequency drops. In this section the elimination of this LF instability of the translation operator will be discussed.

The smoothed translation operator as it was derived in the previous Section (36) has two very peculiar properties. First, the spectrum $t_{n,m}$ is zero whenever $|\, m \,| > |\, n \,|$ or $|\, m \,| > L$ so that when a dot is placed at every nonzero Fourier coefficient an hourglass shaped figure is obtained. Second, the coefficient $t_{n,m}$ contains only Hankel functions of order $|n|$ or lower. These properties are not shared by the translation operators of 2.2 and 2.3. They will enable us to construct a translation operator that remains valid at very low frequencies and even has a DC limit. The drawback is a failure due to numerical roundoff error at HF.

The first part of the derivation entails a further manipulation of the smoothed translation operator. Consider a translation operator defined as follows

$$\widehat{T}(k\mathbf{r}_T,\theta,\phi)=\sum_{n=0}^{L_d}\sum_{m=-L}^{L}2s_nt_{n,m}e^{jn\theta}e^{jm\phi}. \tag{42}$$

Note that the summation over n starts at 0 instead of $-L_d$. We will call $\widehat{T}(k\mathbf{r}_T,\theta,\phi)$ the triangular translation operator, since its spectrum is more or less triangle shaped. It is easily seen that this translation operator is a valid one for use in (20) since the plane wave $e^{-j\mathbf{k}(\theta,\phi)\cdot\mathbf{r}_A}$ is invariant under the transformation $(\theta,\phi)\to(2\pi-\theta,\phi+\pi)$ and $(-1)^mt_{-n,m}=t_{n,m}$

$$\frac{1}{4\pi}\int_0^{2\pi}\int_0^{2\pi}e^{-j\mathbf{k}(\theta,\phi)\cdot\mathbf{r}_A}\widehat{T}(k\mathbf{r}_T,\theta,\phi)\mathrm{d}\theta\mathrm{d}\phi \tag{43}$$

$$=\frac{1}{4\pi}\int_0^{2\pi}\int_0^{2\pi}e^{-j\mathbf{k}(\theta,\phi)\cdot\mathbf{r}_A}\sum_{n=0}^{L_d}\sum_{m=-L}^{L}t_{n,m}e^{jn\theta}e^{jm\phi}\mathrm{d}\theta\mathrm{d}\phi \tag{44}$$

$$+\frac{1}{4\pi}\int_0^{2\pi}\int_0^{2\pi}e^{-j\mathbf{k}(\theta,\phi)\cdot\mathbf{r}_A}\sum_{n=1}^{L_d}\sum_{m=-L}^{L}t_{n,m}e^{jn\theta}e^{jm\phi}\mathrm{d}\theta\mathrm{d}\phi, \tag{45}$$

$$=\frac{1}{4\pi}\int_0^{2\pi}\int_0^{2\pi}e^{-j\mathbf{k}(\theta,\phi)\cdot\mathbf{r}_A}\sum_{n=0}^{L_d}\sum_{m=-L}^{L}t_{n,m}e^{jn\theta}e^{jm\phi}\mathrm{d}\theta\mathrm{d}\phi \tag{46}$$

$$+\frac{1}{4\pi}\int_0^{2\pi}\int_0^{2\pi}e^{-j\mathbf{k}(\theta,\phi)\cdot\mathbf{r}_A}\sum_{n=-L_d}^{-1}\sum_{m=-L}^{L}(-1)^mt_{-n,m}e^{jn\theta}e^{jm\phi}\mathrm{d}\theta\mathrm{d}\phi, \tag{47}$$

$$=\frac{1}{4\pi}\int_0^{2\pi}\int_0^{2\pi}e^{-j\mathbf{k}(\theta,\phi)\cdot\mathbf{r}_A}\widetilde{T}(k\mathbf{r}_T,\theta,\phi)\mathrm{d}\theta\mathrm{d}\phi. \tag{48}$$

The second part of the derivation of LF-stable translation operators consists of shifting the integration path along the θ direction into the complex plane

$$h_0^{(2)}(kr)\approx\frac{1}{4\pi}\int_0^{2\pi}\int_{j\chi}^{2\pi+j\chi}e^{-j\mathbf{k}(\theta,\phi)\cdot\mathbf{r}_A}\widehat{T}(k\mathbf{r}_T,\theta,\phi)\mathrm{d}\theta\mathrm{d}\phi. \tag{49}$$

Fig. 2 shows the old and new integration paths, i.e. C_0 and C_2, respectively. The integrated function is analytical, hence the contributions from C_0 and $C_1+C_2+C_3$ are equal. The integrated function is also periodic with period 2π, hence the contributions from C_1 and C_3 cancel each other, legitimating the shift in Eq. (49). A shift into the complex plane simply multiplies the Fourier coefficients $2s_nt_{n,m}$ with a factor $e^{-n\chi}$. The two outer sums in (42) can thus still be performed using the FFT algorithm. A side effect of the complex shift is that the symmetry of the plane wave under the transformation $(\theta,\phi)\to(2\pi-\theta,\phi+\pi)$ can no longer be used to reduce the number of points in a radiation pattern. Indeed, $(\theta+j\chi,\phi)$ maps into $(2\pi-\theta-j\chi,\phi+\pi)$ which is not a point in the integration domain.

In order to make Eq. (49) numerically stable for low frequencies, the complex shift must be tailored to compensate the divergent behavior of the spectrum of the triangular translation operator. In [12], a similar problem is encountered. However, only translations in the z-direction were stabilized. For this special case, the value of χ was chosen by imposing the condition that, after the application of the complex shift, no Fourier coefficient (of the translation operator) should have a magnitude larger than the magnitude of the lowest order coefficient $t_{0,0}$. The aim of this was to avoid that the highest order coefficients, which contribute the least in the addition theorem, numerically overwhelm the low order terms. A similar reasoning will be applied here, with the generalization that the selected value of χ must work for all translation directions. We propose the following algorithm for calculating χ:

1: Calculate $2s_nt_{n,m},\forall n\in[0,L_d],m\in[-L,L]$ for a translation vector $\mathbf{r}_T=r_T^{\min}\hat{\mathbf{e}}_x$.
2: Determine the maximum over all m: $t_n=\max_m(|2s_nt_{n,m}|),\forall n\in[0,L_d]$.
3: $\chi=0$
4: **repeat**
5: Determine $n_{\max}$ such that $|t_{n_{\max}}|\geqslant|t_n|,\forall n\in[0,L_d]$
6: **if** $n_{\max}=0$ **then**
7: $\delta=0$
8: **else**
9: $\delta=\frac{1}{n_{\max}}\ln|\frac{t_{n_{\max}}}{t_0}|$
10: **end if**
11: $t_n=e^{-n\delta}t_n,\forall n\in[0,L_d]$
12: $\chi=\chi+\delta$
13: **until** $|\delta|<\tau$
14: **return** χ

with τ a small number (e.g. 10^{-12} in double precision), for determining whether $|\delta|$ is close enough to zero. Upon termination this algorithm yields a complex shift that is suitable for all translations in the xy-plane, since the chosen translation direction

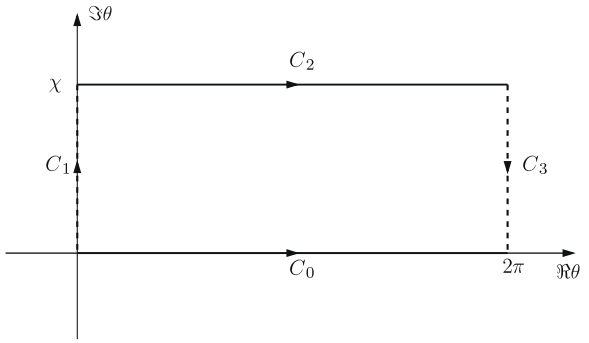

Fig. 2. Shifting the integration path C_0 into the complex plane. The new integration path is C_2.

is $\hat{\boldsymbol{e}}_x$ and $|2s_n t_{n,m}|$ does not depend on ϕ_T. It can, however, also be used for the other translation directions. This can be understood by means of the same argument as the one used for the calculation of L_d. The translations in the *xy*-plane usually have the Fourier coefficients with the largest magnitude, hence the value of χ obtained by means of the algorithm can be used for the other translations too. Although this argument is tenuous and does not actually prove that the selected χ also works for translation directions that are neither close to the *xy*-plane nor to the *z*-axis, numerical experiments (see Section 6) indicate that it is at least approximately valid.

The translation distance used in the algorithm is $r_T^{\min}$. The superscript min is introduced to indicate that the shortest translation distance should be used. If (49) is used in an MLFMA-like algorithm, many different translation distances are encountered. As was explained in [12], the shortest used translation distance should in this case be used in the calculation of χ. This rule stems from the fact that the shortest translation requires the most near-field information. Therefore, if χ is adequate for the shortest translation, the longer translations should also be accurate.

5. Transitions between levels

In a full multilevel scheme, a procedure must be devised for calculating the radiation pattern of a box on level $p+1$ from the radiation patterns of its child boxes on level p. In the usual MLFMA this procedure boils down to an interpolation of the radiation pattern. The transposed procedure, corresponding to an anterpolation in the usual MLFMA, is required while going down in the tree. The method proposed here has, in the LF case, an almost constant number of samples. However, procedures similar to inter- and anterpolations are still necessary because the value of the complex shift χ changes between levels. We will call these the extrapolations, since the integration domains $[0,2\pi]\otimes[0,2\pi]+j\chi_p$ and $[0,2\pi]\otimes[0,2\pi]+j\chi_{p+1}$ are disjoint, where χ_p is the value of the complex shift on level p. As was noted in [6], these extrapolations can be done using the FFT algorithm. However, this turned out to be significantly less accurate than a procedure based on least-squares fits. The least-squares technique, however, has the disadvantage that dense matrices need to be multiplied. In the following we will propose an modified FFT based method that allows accurate extrapolations. This allows for a very efficient transition between the levels.

Let $\Psi(\theta+j\chi_p,\phi)$ be the radiation pattern of a box on level p, discretized with $2L_d^p+1$ points in θ and ϕ. Then the extrapolation starts with the calculation, by means of FFT, of the spectrum of $\Psi(\theta+j\chi_p,\phi)$

$$\Psi(\theta+j\chi_p,\phi)=\sum_{n=-L_d^p}^{L_d^p}\sum_{m=-L_d^p}^{L_d^p}c_{n,m}e^{jn\theta-n\chi_p}e^{jm\phi}=\sum_{n=-L_d^p}^{L_d^p}\sum_{m=-L_d^p}^{L_d^p}d_{n,m}^p e^{jn\theta}e^{jm\phi} \tag{50}$$

The spectrum $c_{n,m}$ can be seen as the spectrum of $\Psi(\theta,\phi)$. Because $\Psi(\theta,\phi)=\Psi(2\pi-\theta,\phi+\pi)$, this spectrum satisfies the following property

$$c_{n,m}=(-1)^m c_{-n,m}. \tag{51}$$

Also, $d_{n,m}^p=c_{n,m}e^{-n\chi_p}$. This means that the spectrum $d_{n,m}^p$ of $\Psi(\theta+j\chi_p,\phi)$ has a large magnitude for negative n and a small magnitude for positive n. From this it immediately follows that $d_{|n|,m}^p$ is known with much less accuracy than $d_{-|n|,m}^p$. It now turns out that changing χ actually amplifies these errors. Indeed, the effect of the changing the complex shift from χ_p to χ_{p+1} is that the spectrum $d_{n,m}^p$ is multiplied with $e^{n(\chi_p-\chi_{p+1})}$. Since $\chi_p>\chi_{p+1}$, this blows up the small $d_{n,m}^p$ and shrinks the large $d_{n,m}^p$. Hence the large relative error on the small coefficients is amplified as well. This can be avoided by explicitly using the symmetry relation (51), leading to the following formula

$$d_{n,m}^{p+1}=\begin{cases} n\leqslant 0: d_{n,m}^p e^{n(\chi_p-\chi_{p+1})} \\ n>0: (-1)^m d_{-n,m}^p e^{-n(\chi_p+\chi_{p+1})} \end{cases} \tag{52}$$

In this way, the entire spectrum of $\Psi(\theta+j\chi_{p+1},\phi)$ is calculated from $d_{n,m}^p$ with negative n. Hence they are known with a good accuracy. The radiation pattern on level $p+1$ can then be obtained by means of FFTs.

When going down in the tree, the transposed extrapolation must be used. This transpose can be taken by writing all operations (FFTs, calculation of $d_{n,m}^{p+1}$ with (52)) as the multiplication of a matrix and taking the transpose of the entire product. The computational cost of this procedure is the same as the original extrapolation, since the Fourier matrix is its own transpose.

6. Numerical results

6.1. Single level results

In the previous sections, a closed form expression for the translation operator was derived, as well as a way to determine the parameters L, L_d and χ. In this section we will investigate how well this ensemble of methods works. All calculations were carried out in Matlab, in double precision. In the first test the frequency is varied for a fixed configuration of boxes. The used configuration is the one seen in Fig. 1, except that there are sources on all the vertices $\boldsymbol{R}_1 - \boldsymbol{r}_a^p$ of box 1 and receivers on all the vertices $\boldsymbol{R}_2 - \boldsymbol{r}_d^q$ of box 2. The 64 interactions are all calculated both directly and using the addition theorem. The maximum relative error (over the 64 interactions) is then calculated as

$$\Delta = \max_{pq} \left| \frac{\pi \sum_{n_\theta=1}^{N_\theta} \sum_{n_\phi=1}^{N_\phi} \widehat{T}(k\boldsymbol{r}_T, \theta_{n_\theta} + j\chi, \phi_{n_\phi}) e^{-j\boldsymbol{k}(\theta_{n_\theta}+j\chi,\phi_{n_\phi})\cdot(\boldsymbol{r}_T+\boldsymbol{r}_a^p-\boldsymbol{r}_d^q)}}{N_\theta N_\phi h_0^{(2)}(k|\boldsymbol{r}_T + \boldsymbol{r}_a^p - \boldsymbol{r}_d^q|)} - 1 \right|. \tag{53}$$

The sides of the boxes are 1 m. The maximum relative error is shown in Fig. 3, for various target accuracies ϵ. It can be seen that the error is always below the target acuracy, except for the rightmost points on the curve with target accuracy 10^{-8}. This failure can be traced back to the HF-breakdown of the addition theorem. This breakdown is seen earliest in the highest-accuracy curve because both L is higher and smaller errors are visible. However, at the highest shown frequency the boxes have a side of 1.6 wavelengths, which is already quite large for a method which is essentially HF unstable. For comparison, Fig. 4 shows the maximum relative error is when the usual MLFMA is used. It is clear that the MLFMA is not error controllable for LF. However, for not too high accuracies, the error-controllability regions of the MLFMA and the novel method overlap. This opens up the possibility of making a switch to the MLFMA with uniform discretization, once the boxes reach a certain size, yielding a broadband method. It is worthwhile to point out that increasing the number of buffer boxes (the boxes that are considered too near to be treated with the addition theorem on a certain level) increases the size of the overlap. Also, increasing the number of buffer boxes allows an overlap to be found for higher accuracies. Further discussion of this overlap falls outside the scope of this contribution.

The results shown in Fig. 3 demonstrate that the proposed mechanisms for determining L, L_d and χ are adequate if used for one translation. In the second test we will show that these parameters also work when many different translations have

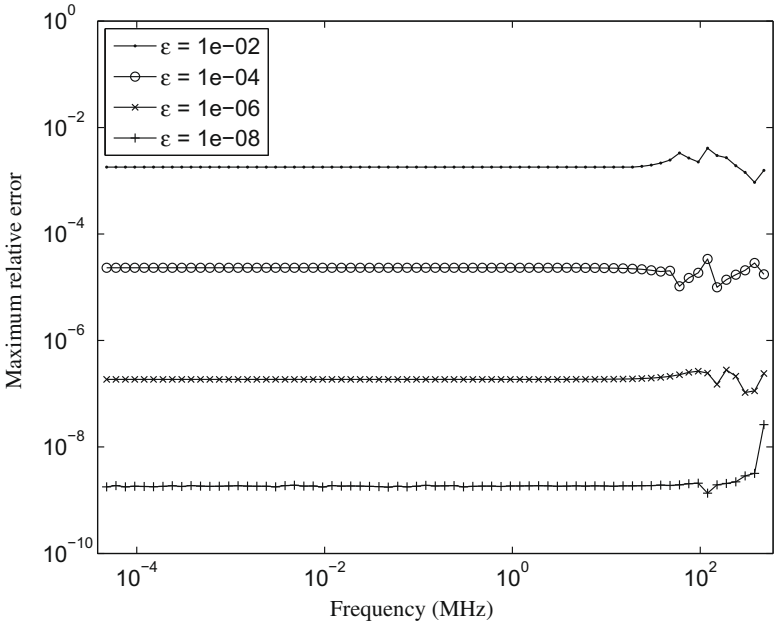

Fig. 3. The maximum relative error Δ as a function of frequency.

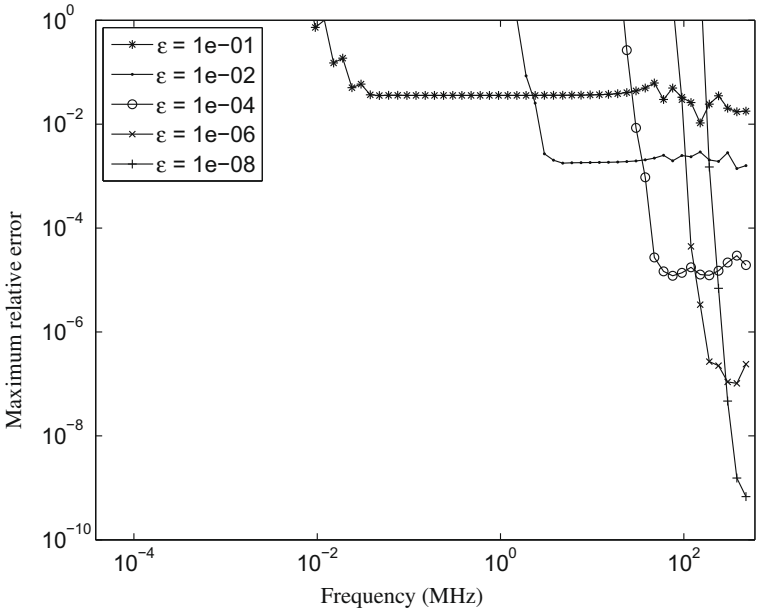

Fig. 4. The maximum relative error Δ as a function of frequency for the MLFMA.

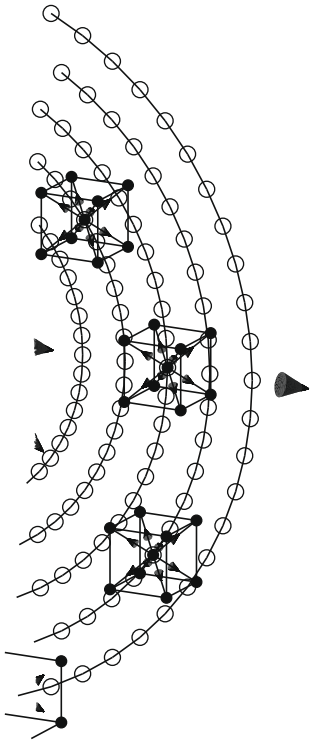

to be performed, as is the case in an FMM. Since the calculation of both L_d and χ was based on translations in the xy-plane, we will be mostly interested in the error-controllability of the method for θ_T differing much from $\frac{\pi}{2}$. The translations under consideration are therefore defined by the following formula

$$\boldsymbol{r}_T = r_T^{\min}\left(1+\frac{n_r}{4}\right)\left[\sin\left(\frac{\pi n_t}{30}\right)\hat{\boldsymbol{e}}_x + \cos\left(\frac{\pi n_t}{30}\right)\hat{\boldsymbol{e}}_z\right], \quad \forall n_r \in [0,4], n_t \in [0,30]. \tag{54}$$

and shown in Fig. 5. A further reason to omit a dependence on ϕ_T is that the values of L_d and χ do not depend on ϕ_T, even if we would use a general translation operator in the xy-plane for their calculation. In addition, both the simple dependence on ϕ_T of the translation operator and numerical tests indicate that the error is relatively invariant under rotations around the z-axis. The accuracy results are summarized in Fig. 6a and b. For both figures the target accuracy was 10^{-5}, the sides of the boxes were 1 m and the shortest translation distance $r_T^{\min}$ was 3 m. The frequency for Fig. 6a was 4.77 kHz, while the frequency for Fig. 6b was 239 MHz. This leads to the parameters $L = 20$, $L_d = 21$ and $\chi = 11.51098$ for Fig. 6a and $L = 24$,

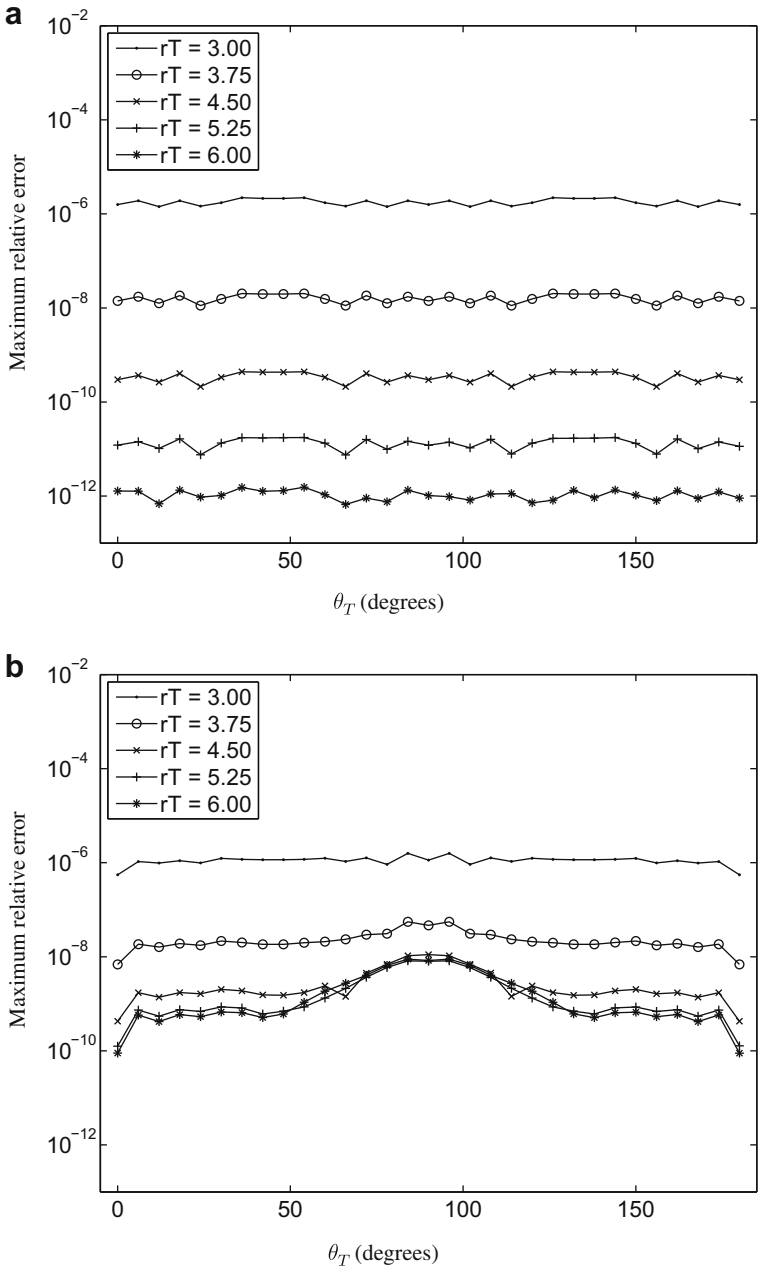

Fig. 6. The maximum relative error as a function of θ_T.

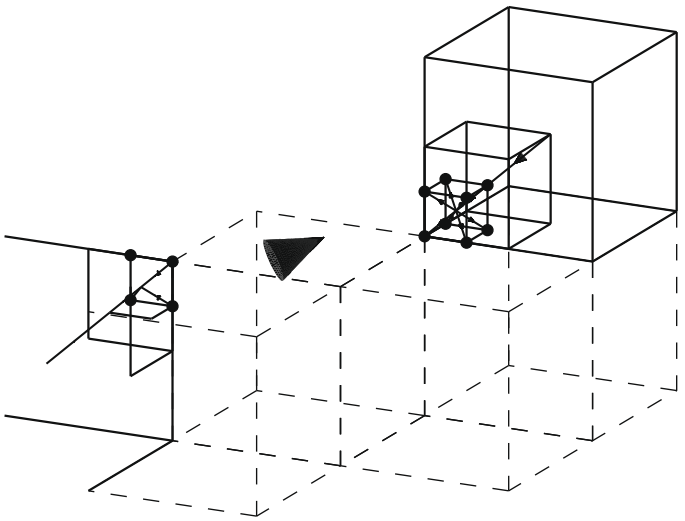

$L_d = 32$ and $\chi = 1.03578$ for Fig. 6b. From these figures, it is clear that the accuracy requirements are fulfilled for all the tested translations. Therefore, this validates the heuristic algorithms devised for calculating L_d and χ and shows the usefulness of the new addition theorem in an FMM.

6.2. Multi level results

The extrapolation procedure outlined in Section 5 and its transpose were also implemented in Matlab and tested on a geometry as shown in Fig. 7. The largest boxes have sides 1 m, the frequency is 477 MHz and the target accuracy is 10^{-6}. The largest boxes are divided $n_{\text{level}} - 1$ times and the error of the addition theorem is again calculated as the maximum error over the 64 combinations of vertices. Table 1 shows the obtained accuracy for various numbers of levels. These results clearly demonstrate the error-controllability of the total algorithm.

7. Conclusion

A novel plane wave addition theorem has been presented. It was constructed by judiciously replacing spherical harmonics in the translation operator of the MLFMA with pseudospherical harmonics. Although these novel distributions have a diverging Fourier spectrum, truncation of the spectrum yields a finite and valid translation operator. However, the divergence of the spectrum makes it impossible to choose the truncation bound arbitrarily large, leading to an HF numerical instability. A fast algorithm for calculating the Fourier spectrum has been provided. For LF, the specific form of the Fourier spectrum of the pseudospherical harmonics has allowed us to find a complex shift that is capable of compensating most of the divergence of the spherical Hankel function, thereby eliminating the LF instability. In addition, the transitions between levels can be done very efficiently using FFTs. To the best knowledge of the authors, this is the first analytically known plane wave addition theorem that is numerically stable in the quasi static regime. Moreover, the numerical results show that it is error controllable for sufficiently high frequencies. Therefore a hybrid method with the usual MLFMA is straightforward, yielding a broadband method.

Acknowledgement

The work of I. Bogaert was supported by a doctoral grant from the Institute for the Promotion of Innovation through Science and Technology in Flanders (IWT-Vlaanderen).

Appendix A. The spherical harmonics

The Legendre polynomials $P_l(x)$ are defined as

$$P_l(x) = \frac{1}{2^l l!}\frac{\mathrm{d}^l}{\mathrm{d}x^l}(x^2-1)^l, \tag{55}$$

The spherical harmonics $Y_{l,m}(\theta,\phi)$ used in this paper are defined as

$$Y_{l,m}(\theta,\phi) = K_{l,m}e^{jm\phi}\frac{\sin^m\theta}{2^l l!}\left(\frac{1}{\sin\theta}\frac{\mathrm{d}}{\mathrm{d}\theta}\right)^{l+m}\sin^{2l}\theta, \tag{56}$$

with integers l and m so that $l \in [0,\infty]$ and $m \in [-l,l]$. Furthermore

$$K_{l,m} = \sqrt{\frac{2l+1}{4\pi}\frac{(l-m)!}{(l+m)!}}. \tag{57}$$

Using (56), the following properties of the spherical harmonics of real arguments are easily proven:

$$(-1)^m Y_{l,-m}(\theta,\phi) = Y^*_{l,m}(\theta,\phi), \tag{58}$$

$$Y_{l,m}(\pi-\theta,\phi+\pi) = (-1)^l Y_{l,m}(\theta,\phi), \tag{59}$$

$$Y_{l,m}(2\pi-\theta,\phi+\pi) = Y_{l,m}(\theta,\phi). \tag{60}$$

The spherical harmonics satisfy the following orthogonality relation

$$\int_0^{2\pi}\int_0^{\pi} Y_{l_1,m_1}(\theta,\phi)Y^*_{l_2,m_2}(\theta,\phi)\sin\theta\mathrm{d}\theta\mathrm{d}\phi = \delta_{l_1,l_2}\delta_{m_1,m_2}. \tag{61}$$

Also, the spherical harmonics satisfy

$$P_l(\cos\gamma) = \frac{4\pi}{2l+1}\sum_{m=-l}^{l} Y^*_{l,m}(\theta_1,\phi_1)Y_{l,m}(\theta_2,\phi_2), \tag{62}$$

with

$$\cos\gamma = \cos\theta_1\cos\theta_2 + \sin\theta_1\sin\theta_2\cos(\phi_1-\phi_2). \tag{63}$$

Appendix B. The pseudospherical harmonics

The so-called pseudospherical harmonics $U_{l,m}(\theta,\phi)$ used in this paper are defined as

$$U_{l,m}(\theta,\phi) = K_{lm}e^{jm\phi}\frac{\sin^m\theta}{2^l l!}\left(\frac{1}{\sin\theta}\frac{\mathrm{d}}{\mathrm{d}\theta}\right)^{l+m}[S(\theta)\sin^{2l}\theta], \tag{64}$$

with $S(\theta) = \frac{|\sin\theta|}{\sin\theta}$ a piecewise constant function that has value $+1$ for $\theta \in]0,\pi[$ and has value -1 for $\theta \in]\pi,2\pi[$. The derivatives in (64) must be interpreted in a distributional sense, since $U_{l,m}(\theta,\phi)$ contains Dirac delta distributions and derivatives thereof. Therefore the pseudospherical harmonics only have meaning when they are integrated with sufficiently smooth functions.

The following properties of the pseudospherical harmonics are very similar to properties (59) and (60) of the spherical harmonics

$$U_{l,m}(\pi-\theta,\phi+\pi) = (-1)^l U_{l,m}(\theta,\phi), \tag{65}$$

$$U_{l,m}(2\pi-\theta,\phi+\pi) = -U_{l,m}(\theta,\phi). \tag{66}$$

However, property (58) nor an orthogonality relation like (61) exist for the pseudospherical harmonics. Instead the following orthogonality relation holds

Theorem B.1. *For any integers l_1, l_2 and m_1, m_2 satisfying $l_j \geqslant 0$ and $-l_j \leqslant m_j \leqslant l_j$ the following holds*

$$\int_0^{2\pi}\int_0^{2\pi} U_{l_1,m_1}(\theta,\phi)Y^*_{l_2,m_2}(\theta,\phi)\sin\theta\mathrm{d}\theta\mathrm{d}\phi = 2\delta_{l_1,l_2}\delta_{m_1,m_2}. \tag{67}$$

Proof. To prove this, first replace $Y^*_{l_2,m_2}(\theta,\phi)$ by $(-1)^{m_2}Y_{l_2,-m_2}(\theta,\phi)$ and integrate over ϕ

$$\int_0^{2\pi}\int_0^{2\pi} U_{l_1,m_1}(\theta,\phi)Y^*_{l_2,m_2}(\theta,\phi)\sin\theta \mathrm{d}\theta\mathrm{d}\phi \tag{68}$$

$$= 2\pi\delta_{m1,m2}(-1)^{m_2}\frac{K_{l_1,m_1}}{2^{l_1}l_1!}\frac{K_{l_2,-m_2}}{2^{l_2}l_2!} \tag{69}$$

$$\times\int_0^{2\pi}\left(\frac{1}{\sin\theta}\frac{\mathrm{d}}{\mathrm{d}\theta}\right)^{l_1+m_1}[S(\theta)\sin^{2l_1}\theta]\left(\frac{1}{\sin\theta}\frac{\mathrm{d}}{\mathrm{d}\theta}\right)^{l_2-m_1}[\sin^{2l_2}\theta]\sin\theta\mathrm{d}\theta. \tag{70}$$

Repeated partial integration yields an integral that is well-defined

$$2\pi\delta_{m1,m2}(-1)^{l_1}\frac{K_{l_1,m_1}}{2^{l_1}l_1!}\frac{K_{l_2,-m_2}}{2^{l_2}l_2!}\int_0^{2\pi}S(\theta)\sin^{2l_1}\theta\left(\frac{1}{\sin\theta}\frac{\mathrm{d}}{\mathrm{d}\theta}\right)^{l_2+l_1}[\sin^{2l_2}\theta]\sin\theta\mathrm{d}\theta. \tag{71}$$

The definition of $S(\theta)$ is then used to obtain an integral that is very similar to the orthogonality integral of the spherical harmonics

$$2\pi\delta_{m1,m2}(-1)^{l_1}\frac{K_{l_1,m_1}}{2^{l_1}l_1!}\frac{K_{l_2,-m_2}}{2^{l_2}l_2!}\int_0^{2\pi}\sin^{2l_1}\theta\left(\frac{1}{\sin\theta}\frac{\mathrm{d}}{\mathrm{d}\theta}\right)^{l_2+l_1}[\sin^{2l_2}\theta]|\sin\theta|\mathrm{d}\theta \tag{72}$$

$$= 2\pi\delta_{m1,m2}((-1)^{l_1}+(-1)^{l_2})\frac{K_{l_1,m_1}}{2^{l_1}l_1!}\frac{K_{l_2,-m_2}}{2^{l_2}l_2!}\times\int_0^{\pi}\sin^{2l_1}\theta\left(\frac{1}{\sin\theta}\frac{\mathrm{d}}{\mathrm{d}\theta}\right)^{l_2+l_1}[\sin^{2l_2}\theta]\sin\theta\mathrm{d}\theta \tag{73}$$

$$= (1+(-1)^{l_1+l_2})\int_0^{2\pi}\int_0^{\pi}Y_{l_1,m_1}(\theta,\phi)Y^*_{l_2,m_2}(\theta,\phi)\sin\theta\mathrm{d}\theta\mathrm{d}\phi \tag{74}$$

$$= (1+(-1)^{l_1+l_2})\delta_{l_1,l_2}\delta_{m_1,m_2} = 2\delta_{l_1,l_2}\delta_{m_1,m_2}. \tag{75}$$

This conludes the proof of (67). □

Appendix C. Useful properties of the pseudospherical harmonics

In this appendix, some properties will be proven that are necessary for calculating the Fourier spectrum of the pseudospherical harmonics. The so-called Gamma function $\Gamma(\cdot)$ will be extensively used. The most often used property of this function is $x\Gamma(x)=\Gamma(x+1)$. See chapter 6 in [14] for the definition and more information about the Gamma function. First we will prove the following theorem

Theorem C.1. *For any integer l satisfying $l \geqslant 0$ the following holds*

$$S(\theta)\sin^{2l}\theta = \frac{2(-1)^l\Gamma(2l+1)}{2^{2l}\pi}\sum_{p=0}^{\infty}\frac{\Gamma(p-l+\frac{1}{2})}{\Gamma(p+l+\frac{3}{2})}\sin[(2p+1)\theta] \tag{76}$$

Proof. It is easily verified that the result holds for $l=0$. It then remains to be proven from induction that if (76) is correct for a certain $l \geqslant 0$, it is correct for $l+1$. Therefore the product of the right hand side of (76) with $\sin^2\theta$ must be investigated:

$$\sin^2\theta\frac{2(-1)^l\Gamma(2l+1)}{2^{2l}\pi}\sum_{p=0}^{\infty}\frac{\Gamma(p-l+\frac{1}{2})}{\Gamma(p+l+\frac{3}{2})}\sin[(2p+1)\theta] = \frac{(-1)^l\Gamma(2l+1)}{2^{2l+1}\pi}\sum_{p=0}^{\infty}\frac{\Gamma(p-l+\frac{1}{2})}{\Gamma(p+l+\frac{3}{2})}\times\{2\sin[(2p+1)\theta]$$
$$-\sin[(2p+3)\theta]-\sin[(2p-1)\theta]\}. \tag{77}$$

The factor $\sin^2\theta$ was absorbed using the product formulas for the sine function. We proceed by splitting the result into three separate sums, with the first containing $\sin[(2p+1)\theta]$, the second containing $\sin[(2p+3)\theta]$ and the third containing $\sin[(2p-1)\theta]$. In the second and third sum, the substitutions $p\to p-1$ and $p\to p+1$ are, respectively made. By using the identity

$$\frac{\Gamma(-l+\frac{1}{2})}{\Gamma(l+\frac{3}{2})} = -\frac{\Gamma(-l-\frac{1}{2})}{\Gamma(l+\frac{1}{2})}, \tag{78}$$

the excess term in the third sum can be absorbed into the second sum. The three sums can then again be combined into one sum which is easily simplified to

$$\sin^2\theta\frac{2(-1)^l\Gamma(2l+1)}{2^{2l}\pi}\sum_{p=0}^{\infty}\frac{\Gamma\left(p-l+\frac{1}{2}\right)}{\Gamma\left(p+l+\frac{3}{2}\right)}\sin[(2p+1)\theta]=-\frac{(-1)^l\Gamma(2l+1)}{2^{2l+1}\pi}\sum_{p=0}^{\infty}2(l+1)(2l+1)\frac{\Gamma\left(p-l-\frac{1}{2}\right)}{\Gamma\left(p+l+\frac{5}{2}\right)}\sin[(2p+1)\theta] \tag{79}$$

$$=\frac{2(-1)^{l+1}\Gamma(2(l+1)+1)}{2^{2(l+1)}\pi}\sum_{p=0}^{\infty}\frac{\Gamma\left(p-(l+1)+\frac{1}{2}\right)}{\Gamma\left(p+(l+1)+\frac{3}{2}\right)}\sin[(2p+1)\theta], \tag{80}$$

which concludes the proof. □

Now we move on to proving the wanted equality

Theorem C.2. *For any integers l and m satisfying $l \geqslant 0$ and $-l \leqslant m \leqslant l$ the following holds*

$$\left(\frac{1}{\sin\theta}\frac{\mathrm{d}}{\mathrm{d}\theta}\right)^{l+m}[S(\theta)\sin^{2l}\theta]=\frac{2^{l+m+1}\Gamma(l+1)}{\sqrt{\pi}}\sum_{p=0}^{\infty}\lambda_{l,m}^{p}\sin[(l+m+2p+1)\theta], \tag{81}$$

with

$$\lambda_{l,m}^{p}=\frac{\Gamma\left(p+m+\frac{1}{2}\right)\Gamma(l+m+p+1)}{\Gamma\left(m+\frac{1}{2}\right)\Gamma\left(l+p+\frac{3}{2}\right)\Gamma(p+1)}. \tag{82}$$

Proof. This proof will also be done using induction. By means of Theorem C.1 and

$$\frac{\Gamma(l+1)}{\Gamma\left(-l+\frac{1}{2}\right)}=\frac{(-1)^l\Gamma(2l+1)}{2^{2l}\sqrt{\pi}}, \tag{83}$$

it is easy to prove (81) for the special case $m=-l$. Now assume that (81) holds for a certain $m\in[-l,l[$, then we have to prove that it also holds for $m+1$.

$$\left(\frac{1}{\sin\theta}\frac{\mathrm{d}}{\mathrm{d}\theta}\right)^{l+m+1}[S(\theta)\sin^{2l}\theta] \tag{84}$$

$$=\left(\frac{1}{\sin\theta}\frac{\mathrm{d}}{\mathrm{d}\theta}\right)\frac{2^{l+m+1}\Gamma(l+1)}{\sqrt{\pi}}\sum_{p=0}^{\infty}\lambda_{l,m}^{p}\sin[(l+m+2p+1)\theta] \tag{85}$$

$$=\frac{2^{l+m+1}\Gamma(l+1)}{\sqrt{\pi}\sin\theta}\sum_{p=0}^{\infty}(l+m+2p+1)\lambda_{l,m}^{p}\cos[(l+m+2p+1)\theta]. \tag{86}$$

The factor $(l+m+2p+1)\lambda_{l,m}^{p}$ can be dealt with by means of the following identity

$$(l+m+2p+1)\lambda_{l,m}^{p}=\lambda_{l,m+1}^{p}-\lambda_{l,m+1}^{p-1}. \tag{87}$$

This identity is still valid in the special case where $p=0$ because $\frac{1}{\Gamma(0)}=0$. Equation (85) then becomes

$$\frac{2^{l+m+1}\Gamma(l+1)}{\sqrt{\pi}\sin\theta}\sum_{p=0}^{\infty}(\lambda_{l,m+1}^{p}-\lambda_{l,m+1}^{p-1})\cos[(l+m+2p+1)\theta] \tag{88}$$

$$=\frac{2^{l+m+1}\Gamma(l+1)}{\sqrt{\pi}\sin\theta}\sum_{p=0}^{\infty}\lambda_{l,m+1}^{p}[\cos[(l+m+2p+1)\theta]-\cos[(l+m+2p+3)\theta]], \tag{89}$$

$$=\frac{2^{l+m+2}\Gamma(l+1)}{\sqrt{\pi}}\sum_{p=0}^{\infty}\lambda_{l,m+1}^{p}\sin[(l+m+2p+2)\theta]. \tag{90}$$

which concludes the proof. □

The right hand side of Eq. (81) was based on the right hand side of formula (8.7.1) in [14]. However, to the best knowledge of the authors, Theorem C.2 has never before been stated or proved.

For completeness, the following property of $\lambda_{l,m}^{p}$ will also be shown:

Theorem C.3. *For any x and any integer $p \geqslant 0$, $l \geqslant 0$ and $m\in[-l,l]$ the following holds*

$$\lim_{x\to p}[\lambda_{l,m}^{x}+\lambda_{l,m}^{-x-l-m-1}]=0. \tag{91}$$

Proof. Using the definition (82) for $\lambda_{l,m}^{-x-l-m-1}$ yields

$$\lambda_{l,m}^{-x-l-m-1} = \frac{\Gamma\left(-x-l-\frac{1}{2}\right)\Gamma(-x)}{\Gamma\left(m+\frac{1}{2}\right)\Gamma\left(-x-m+\frac{1}{2}\right)\Gamma(-x-l-m)}, \tag{92}$$

$$= \frac{\sin(\pi(x+l+m))\sin\left(\pi\left(x+m-\frac{1}{2}\right)\right)}{\sin(\pi x)\sin\left(\pi\left(x+l+\frac{1}{2}\right)\right)} \times \frac{\Gamma\left(x+m+\frac{1}{2}\right)\Gamma(l+m+x+1)}{\Gamma\left(m+\frac{1}{2}\right)\Gamma\left(l+x+\frac{3}{2}\right)\Gamma(x+1)}, \tag{93}$$

$$= \frac{\sin(\pi(x+l+m))\sin\left(\pi\left(x+m-\frac{1}{2}\right)\right)}{\sin(\pi x)\sin\left(\pi\left(x+l+\frac{1}{2}\right)\right)}\lambda_{l,m}^{x}. \tag{94}$$

The following form of the functional equation of the Gamma function was used to obtain this result

$$\Gamma(-z)\Gamma(z+1) = -\frac{\pi}{\sin(\pi z)}. \tag{95}$$

By means of Eq. (94), the limit reduces to

$$\lim_{x\to p}[\lambda_{l,m}^{x} + \lambda_{l,m}^{-x-l-m-1}] = \lim_{x\to p}\lambda_{l,m}^{x}\left[1 + \frac{\sin(\pi(x+l+m))\sin\left(\pi\left(x+m-\frac{1}{2}\right)\right)}{\sin(\pi x)\sin\left(\pi\left(x+l+\frac{1}{2}\right)\right)}\right], \tag{96}$$

$$= \lambda_{l,m}^{p}\left[1 + (-1)^{l+m}\frac{(-1)^{p+m+1}}{(-1)^{p+l}}\right] = 0, \tag{97}$$

where we used l'Hôspital's rule. □

Appendix D. A recursive formula

Here we will supply a recurrence formula and an algorithm that can be used for an $\mathcal{O}(L^2)$ calculation of $u_{l,m}^{n}$, with $n, l \in [0, L]$ and m fixed. The values of $u_{l,m}^{n}$ for negative n can be obtained by means of Eq. (23). The recurrence is proven in the following theorem:

Theorem D.1. *For any integer n, $l \geqslant 0$ and $m \in [-l, l]$ the following holds*

$$\frac{2l+1}{2}[\tilde{u}_{l,m}^{n+2} + \tilde{u}_{l,m}^{n}] = (l+m)\tilde{u}_{l-1,m}^{n+1} + (l-m+1)\tilde{u}_{l+1,m}^{n+1}, \tag{98}$$

with $\tilde{u}_{l,m}^{n} = \frac{u_{l,m}^{n}}{K_{l,m}}$.

Proof. We start with the following identity

$$\frac{2l+1}{2}[\lambda_{l,m}^{p+1} + \lambda_{l,m}^{p}] = (l+m)\lambda_{l-1,m}^{p+1} + (l-m+1)\lambda_{l+1,m}^{p}. \tag{99}$$

The proof of this using Eq. (82) is tedious but straightforward. Now we replace p with $\frac{n-l}{2} - q$ to obtain

$$\frac{2l+1}{2}\left[\lambda_{l,m}^{\frac{(n+2)-l}{2}-q} + \lambda_{l,m}^{\frac{n-l}{2}-q}\right] = (l+m)\lambda_{l-1,m}^{\frac{n+1-(l-1)}{2}-q} + (l-m+1)\lambda_{l+1,m}^{\frac{n+1-(l+1)}{2}-q}. \tag{100}$$

Applying the sum operator $\frac{(-j)^m}{2\sqrt{\pi}}\sum_{q=0}^{m+1}(-1)^{m-q}\binom{m+1}{q}$ to this entire equation yields Eq. (98) which concludes the proof. □

For the special case when $n = l - 2$, Theorem 3.1 reduces the recurrence to the simpler form

$$\tilde{u}_{l,m}^{l} = \frac{2(l+m)}{2l+1}\tilde{u}_{l-1,m}^{l-1}. \tag{101}$$

The following algorithm can now be used to calculate all the $\tilde{u}_{l,m}^{n}$ for a fixed m:

```
Calculate ũ^n_{m,m} ∀n ∈ [m, L] and ũ^n_{m+1,m} ∀n ∈ [m+1, L] using the direct formula (28)
for l = m + 2 to L do
    Calculate ũ^l_{l,m} from ũ^{l-1}_{l-1,m} by means of (101)
end for
for h = 0 by 2 to L − m − 4 do
    for l = m + 2 to L − h − 2 do
        n = l + h
        Calculate ũ^{n+2}_{l,m} from ũ^n_{l,m}, ũ^{n+1}_{l-1,m} and ũ^{n+1}_{l+1,m} by means of (98)
    end for
end for
```

References

[1] R. Harrington, Field Computations by Moment Methods, Macmillan, New York, 1968.
[2] L. Gürel, Ö. Ergül, Fast and accurate solutions of extremely large integral-equation problems discretised with tens of millions of unknowns, Electronics Letters 43 (9) (2007) 499–500.
[3] J. Fostier, F. Olyslager, An asynchronous parallel MLFMA for scattering at multiple dielectric objects, IEEE Transactions on Antennas and Propagation 56 (8) (2008) 2346–2355.
[4] M.L. Hastriter, S. Ohnuki, W.C. Chew, Error control of the translation operator in 3D MLFMA, Microwave and Optical Technology Letters 37 (3) (2003) 184–188.
[5] L.J. Jiang, W.C. Chew, Low-frequency fast inhomogeneous plane-wave algorithm (LF-FIPWA), Microwave and Optical Technology Letters 40 (2) (2004) 117–122.
[6] H. Wallen, J. Sarvas, Translation procedures for broadband MLFMA, Progress In Electromagnetics Research (55) (2005) 47–78.
[7] L.J. Jiang, W.C. Chew, A mixed-form fast multipole algorithm, IEEE Transactions on Antennas and Propagation 53 (12) (2005) 4145–4156.
[8] E. Darve, P. Havé, A fast multipole method for Maxwell equations stable at all frequencies, Philosophical Transactions of the Royal Society A 362 (1816) (2004) 603–628.
[9] E. Darve, P. Havé, Efficient fast multipole method for low-frequency scattering, Journal of Computational Physics 197 (1) (2004) 341–363.
[10] H. Cheng, W.Y. Crutchfield, Z. Gimbutas, L.F. Greengard, J.F. Ethridge, J. Huang, V. Rokhlin, N. Yarvin, J. Zhao, A wideband fast multipole method for the Helmholtz equation in three dimensions, Journal of Computational Physics (216) (2006) 300–325.
[11] L. Xuan, A. Zhu, R.J. Adams, S.D. Gedney, A broadband multilevel fast multipole algorithm, in: Proceedings of the IEEE AP-S International Symposium, Monterey, CA, vol. 2, June 2004, pp. 1195–1198.
[12] I. Bogaert, J. Peeters, F. Olyslager, A nondirective plane wave MLFMA stable at low frequencies, IEEE Transactions on Antennas and Propagation, in press.
[13] W. Chew, S. Koc, J. Song, C. Lu, E. Michielssen, A succinct way to diagonalize the translation matrix in three dimensions, Microwave and Optical Technology Letters 15 (3) (1998) 144–147.
[14] M. Abramowitz, I.A. Stegun, Handbook of mathematical functions with formulas, Graphs and Mathematical Tables Advanced, Mathematics, Dover Publications Inc., New York, 1965.
[15] W.C. Chew, J. Jin, E. Michielssen, J. Song, Fast and Efficient Algorithms in Computational Electromagnetics, Artech House, 2001.
[16] J. Sarvas, Performing interpolation and anterpolation entirely by fast Fourier transform in the 3-D multilevel fast multipole algorithm, SIAM Journal on Numerical Analysis 41 (6) (2003) 2180–2196.